Correlation and the density-matrix approach to inelastic electron holography in solid state plasmas

Peter Schattschneider*
Laboratoire MSS-Mat–CNRS-UMR8579, Ecole Centrale Paris, F-92295 Châtenay-Malabry, France

Hannes Lichte
Institute of Structure Physics, Triebenberg-Laboratory, Dresden University, D-01062 Dresden, Germany
(Received 14 May 2004; revised manuscript received 22 September 2004; published 31 January 2005)

Collective excitations in solid state plasmas are a good candidate to measure correlation lengths of conduction electrons. The method of choice seems to be energy filtered electron holography in the transmission electron microscope (TEM) since the interference fringes contain information on the partial coherence of those electrons. Previous experiments showed surprisingly high coherence. We calculate the density-density correlation function in the Al plasma excitation from the dynamic form factor and compare it to results based on similar arguments. For the Al plasma excitation, we find a small extension of $0.1-0.3$ nm over which the movement of charges is correlated. Using the density-matrix formalism, the coherence length of plasmon scattered fast electrons in the TEM is calculated and found to agree with experiment. We show that the small correlation length of conduction electrons does not contradict the coherence length of >10 nm found for fast probe electrons having excited a plasmon in Al. The difference of nearly two orders of magnitude can be traced back to the long-range Coulomb interaction between probe and target electrons. Two unexpected predictions ensue from the present approach: Inelastic holography experiments should show strongly increased contrast of interference fringes *in vacuo*, i.e., outside the specimen, and contrast inversion of fringes in inelastic holograms of very small particles.

DOI: 10.1103/PhysRevB.71.045130 PACS number(s): 71.45.Gm, 34.80.Pa, 82.80.Pv

I. INTRODUCTION

The correlated movement of electrons in matter, as well as coherent superpositions of electron wave functions, play a dominant role for the modeling of energy-loss spectra (e.g., Refs. 1 and 2) and in many quantum applications such as Josephson junctions, quantum tunneling, spintronics, nm-sized semiconductors, nanotubes, and molecules; see, e.g., Refs. 3 and 4. A famous example is the electron correlation in metals. The accurate calculation of the correlation energy in the interacting electron gas is a notorious problem with many approximate solutions and unsatisfactory agreement with experiment. For a review, see, e.g., Ref. 5 and references therein.

It is reasonable to assume that the movement of conduction electrons is correlated over a distance of the order of magnitude of the Thomas-Fermi screening length. On the other hand, the plasmon as a collective excitation is often visualized as an in-phase movement of virtually all conduction electrons in the specimen, thus having infinite correlation length.

In this paper, we set out to describe correlation in solid state plasmas and its relationship to inelastic electron holography by use of the density matrix. As an example, we take Al metal. We first discuss the different existing approaches to a definition of the spatial extension of a plasma excitation. Then we focus on the density-density correlation $p(\mathbf{r})$, i.e., the conditional probability to find an electron a distance $\mathbf{r}$ away from another one. We then show how $p(\mathbf{r})$ relates to the dynamic form factor $S(\vec{\mathbf{Q}},E)$, which in turn is accessible by inelastic scattering experiments with fast electrons. Realizing that the inelastic scattering cross section for fast electrons is closely related to the mutual coherence of the scattered electrons, we are then in a position to elaborate the relationship between $p(\mathbf{r})$ and the mutual object transparency introduced by Rose and co-workers.[6] We can then reanalyze the inelastic interference experiments of Lichte and co-workers. We find that the large coherence length determined experimentally is precisely predicted by theory, and that this is consistent with the small correlation length in solid state plasmas. We predict some peculiar properties of the mutual coherence function and propose new holographic experiments as a test of the present predictions.

II. THE DENSITY CORRELATION FUNCTION

The density correlation $p(\mathbf{r})$ is defined in terms of the density operator $n(\mathbf{r})=\Sigma_{\mathbf{i}}\delta^3(\hat{\mathbf{r}}_{\mathbf{i}}-\mathbf{r})$ as the integral over the expectation value

$$p(\mathbf{r}) = \int d^3r' \langle n(\mathbf{r}')n(\mathbf{r}+\mathbf{r}')\rangle, \tag{1}$$

where the sum is over all particles.

This definition can be extended to time-dependent correlations as

$$p(\mathbf{r},t) = \int d^3r' \langle n(\mathbf{r}',0)n(\mathbf{r}+\mathbf{r}',t)\rangle, \tag{2}$$

where we have assumed that the system is invariant under time translation operations. The frequency component ω of

 ©2005 The American Physical Society

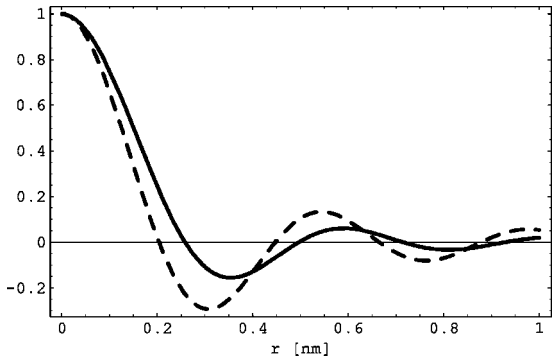

FIG. 1. Density autocorrelation function of Al plasma excitation. Full line: Eq. (4); dashed line: projection onto plane of observation, Eq. (5).

this function is the density correlation function $p_E(\mathbf{r})$ of an excitation of energy $E=\hbar\omega$ in the system

$$p_E(\mathbf{r}) = FT_t[p(\mathbf{r},t)].$$

Here and in the following, we use the abbreviation $FT_x[f(x)]$ for the Fourier transform of a function with respect to the variable x.

Applying the Wiener-Khinchin theorem, $p_E(\mathbf{r})$ is the Fourier transform of the dynamic form factor (see, e.g., Ref. 7) $S(\mathbf{Q},E)$ of the scatterer

$$p_E(\mathbf{r}) = FT_{\mathbf{Q}}[S(\mathbf{Q},E)]. \tag{3}$$

Experimentally, the inelastic electron scattering cross section for cubic systems is isotropic and to a good approximation a Lorentzian in wave-number transfer q with cutoff q_c. This is consistent with the dipole approximation for the dynamic form factor $S(\mathbf{Q},E)\propto\mathbf{Q}^2$ up to the cutoff wave number.

In the dipole approximation, the Fourier transform Eq. (3) can be performed directly,

$$\begin{aligned} p_E(r) &= 2\pi\int_{q_e}^{q_c}\mathbf{Q}^2 S(\mathbf{Q},E)d\mathbf{Q}\int_0^{\pi} d\vartheta\,\sin(\vartheta)e^{i\mathbf{Q}r\,\cos(\vartheta)} \\ &= 4\pi\int_{q_e}^{q_c}\mathbf{Q}^4\frac{\sin(\mathbf{Q}r)}{\mathbf{Q}r}d\mathbf{Q}, \end{aligned} \tag{4}$$

where we have used the fact that no wave-number transfer less than the characteristic transfer $q_e=k_0E/2E_0$ can occur.

In the electron microscope, spatial information is only available projected onto the image plane with coordinates $\mathbf{x}$ (which corresponds to the subspace in reciprocal space subtended by the diffraction plane). When comparing predictions with experimental results, one is rather interested in the z-projected correlation function $\bar{p}=\int p(\mathbf{r})dz$. This is the two-dimensional Fourier transform with respect to the coordinates $\mathbf{q}$ in the diffraction plane—for definition see after Eq. (9). In the dipole approximation with cutoff q_c, this is[8]

$$\begin{aligned} \bar{p}_E(\mathbf{x}) &= FT_{\mathbf{q}}[S(\mathbf{Q},E)] = \int_0^{qc} S(\mathbf{Q},E)e^{i\mathbf{q}\cdot\mathbf{x}}d^2q \\ &= 2\pi\int_0^{qc} S(\mathbf{Q},E)e^{iqx\,\cos(\varphi)}qdqd\varphi \\ &= 2\pi\int_0^{qc}(q_e^2+q^2)J_0(qx)qdq. \end{aligned} \tag{5}$$

Results are shown for Al, compared to the three-dimensional correlation function, in Fig. 1. The 3D correlation function has its first zero at 0.25 nm and its first subsidiary minimum at 0.35 nm with less than 20% probability.

III. VARIOUS APPROACHES TO CORRELATION

According to strong screening in metals, both the correlation length of conduction electrons and the extension of the exchange-correlation hole[9] can be expected to be of the same magnitude as the Thomas-Fermi screening length (some angstroms).

This is consistent with the findings of Egri,[10,11] who derived an extension of ≈0.2 nm for the plasmon in metals and semiconductors from the analysis of what he termed the plasmon wave function. The same order of magnitude is found for the pair distribution function in a coherent superposition of electron-hole excitations.[12] A classical argument suggests to define the extension of the plasmon as the product of the lifetime and the group velocity. For Al, this was found to be 0.4 nm.[13] This last value seems to be in agreement with early experiments on the spatial resolution in plasmon filtered images.[14]

However, more recently Lichte and co-workers[15–17] reported interference experiments with fast electrons having excited a plasmon in Al. Contrary to the predictions, they found a coherence length of almost 10 nm, later on 30 nm from fringe contrast in the inelastic hologram.

This seems to be contradicted by the uncertainty principle: the coherent extension of a plasmon scattered electron in the electron microscope is by definition $\delta x=\hbar/\sqrt{\langle\delta q^2\rangle}$. Since the angular scattering distribution is proportional to a Lorentzian $(q_e^2+q^2)^{-1}$ the variance of which is infinite, the coherence length of the scattered electron comes out as $\delta x=0$.

In the following, we discuss the various approaches more precisely. We shall see that the intuitive argument based on the angular scattering distribution is not far from reality.

A. Mean free path of the excited plasmon

Cheng[13] calculated what he called the localization distance of the excitation as the product of group velocity with the relaxation time. The former was taken to be an average over the observable wave numbers, and the latter was obtained from the energy full width at half maximum (FWHM) of the plasmon peak. The result was 0.4 nm. In fact, what was computed was the mean free path of the plasmon. This need not be the correlation length, as becomes evident when one thinks of solitons which travel over much longer dis-

tances than their spatial extension. In Ref. 13, the puzzling observation can be found that from the angular distribution of scattering, a localization distance of 23 nm can be derived,[38] in disagreement with the experimentally observed spatial resolution of 0.4 nm. The situation is confusing since three different quantities are compared there. Intuitively it is felt that they are related to each other in some way, but it is not clear how.

B. Exchange hole

In the Hartree-Fock approximation for N electrons, the density correlation is

$$p(\mathbf{r}) = \delta^3(\mathbf{r}) + \frac{(N-1)}{v}[1 - g(k_F r)] \tag{6}$$

with the exchange hole[9]

$$g(r) = -\frac{9\{-[k_F r \cos(k_F r)] + \sin(k_F r)\}^2}{2k_F r^6}.$$

g is a universal function of the dimensionless variable $k_F r$, where k_F is the Fermi wave number. This hole describes the tendency of fermions to avoid each other according to the Pauli principle. When, additionally, the electrons are allowed to interact, the Coulomb repulsion will increase the extension of the hole.[9] The size of this repulsion area around an electron gives a clue to the correlation length of electrons in the excited state. It turns out to be close to the screening length for electrostatic perturbations, which in turn equals roughly the average distance of electrons in the gas. For Al, this is 0.107 nm, and we find a FWHM of this hole of 0.1 nm and the first zero is at 0.23 nm.

C. Pair distribution function in correlated electron excitations

In 1957, Ferrell and Quinn[12] explained the high energy of the plasma excitation in a metal with the positional correlation of electrons in the excited state. These correlations stem from coherent superpositions of excited single-electron states with the same relative phase. The pair distribution function of electrons in this excited state with wave vector $\mathbf{k}$ is $\propto\cos(\mathbf{k}\cdot\mathbf{x})$.[12] Averaging over directions yields the density-density correlation function

$$p(r) = \frac{\sin(kr)}{kr}. \tag{7}$$

For k we take the mean wave number $\bar{k}$ of a plasma excitation. Assuming that all q values from 0 to the cutoff wave number q_c are equiprobable, we obtain $\bar{k}=3q_c/4$. The FWHM is 0.16 nm, the first zero at 0.28 nm.

D. Electron-hole distance

An alternative approach to the correlation length starts from the plasmon wave function,[10] defined as the probability amplitude of finding electron-hole pairs separated by $\mathbf{r}$. In a way, this is the opposite of Ferrell's approach because, if the probability of finding two electrons at a distance is high, there will be a low chance to find a hole at the same distance. The result for small k and $\mathbf{r}$ perpendicular to $\mathbf{k}$ is a universal function of the dimensionless parameter $k_F r$,

$$\varphi(k_F r) = \frac{2J_1(k_F r)}{k_F r}. \tag{8}$$

For $\mathbf{r}$ parallel to $\mathbf{k}$, the extension of the wave function is bigger by a factor of roughly 2.2. Averaging over both values, the resulting FWHM is 0.14 nm, and the first zero is at 0.35 nm.

Several values for the extension of the plasma excitation in Al metal are collected in Table I. It can be seen that the various approaches yield very similar values for the correlation length of electrons in metals.

TABLE I. Electron correlation in the Al plasma. The table lists several parameters of the distribution functions (values in nm) as defined in the text. The holography experiment yielded 10% fringe contrast at a shear of 10 nm.

Method	HWHM	First zero	First minimum
Uncertainty principle	0		
$p_E(x)$—Eq. (5)	0.13	0.20	0.30
$p_E(r)$—Eq. (4)	0.16	0.25	0.36
Exchange hole[a]	0.10	0.23	0.23
Pair distribution[b]	0.16	0.28	0.38
Electron-hole distance[c]	0.14	0.35	0.46
Mean free path[d]	0.4		
Holography[e]		10	

[a]Reference 9.
[b]Reference 12.
[c]Reference 10.
[d]Reference 13.
[e]Reference 16.

IV. INELASTIC ELECTRON SCATTERING

In the single scattering approximation, the dynamic form factor S of a scattering medium relates to the double differential inelastic scattering cross section for fast electrons as[7]

$$\frac{\partial^2\sigma}{\partial E\,\partial\Omega} = \frac{4\gamma^2}{a_0^2}\frac{k}{k_0}\frac{S(\mathbf{Q},E)}{Q^4}, \tag{9}$$

where $a_0=4\pi\varepsilon_0\hbar^2/me^2$ is the Bohr radius, and γ is a relativistic factor. We used the three-dimensional vector in reciprocal space,

$$\mathbf{Q} = \begin{pmatrix} \mathbf{q} \\ \mathbf{Q}_E \end{pmatrix}.$$

$q_E=k-k_0$ is the negative difference of radii of the Ewald spheres before and after inelastic scattering. For small energy losses $E \ll E_0$ we have approximately $q_E=-k_0E/2E_0$. Equation (9) is valid in the first Born approximation for an incident plane wave, and for single scattering.

Experimentally, the angular scattering distribution is well approximated by a Lorentzian behavior up to a cutoff angle

θ_c. Therefore, the dynamic form factor in Eq. (9) must be proportional to Q^2 up to $\sqrt{q_E^2+k_0^2\theta_c^2}$. This is the dipole approximation which is often used for ionization edges.[8]

There is an intimate relationship between the double differential scattering cross section Eq. (9) and the density matrix $\rho_E(\mathbf{q},\mathbf{q}')$ of the probe electron after inelastic scattering with energy loss E in the diffraction plane: the former is proportional to the diagonal element of the latter.

The propagation of the probe electron's density matrix in a medium is described by the kinetic equation.[18] The kernel of this integral equation is the mutual object transparency.[6] When Bragg scattering can be neglected and the specimen is thinner than a mean free path for inelastic scattering (which is roughly 100 nm–200 nm for 200 keV incident energy for plasma excitations, and much higher for ionization), the single inelastic scattering approximation applies,[8] and we obtain

$$\rho_E(\mathbf{q},\mathbf{q}') = \left(\frac{me^2\pi}{\varepsilon_0\hbar^2 k}\right)^2 \frac{S(\mathbf{Q},\mathbf{Q}',E)}{Q^2 Q'^2}. \tag{10}$$

The quantity $S(\mathbf{Q},\mathbf{Q}',E)$ on the right-hand side is the mixed dynamic form factor.[19] Equation (9) is a special case of Eq. (10) for $\mathbf{q}=\mathbf{q}'$. Multiple plasmon scattering is thought to be almost incoherent and would probably not affect the coherence length but rather the incoherent background in the diffraction plane. Even this will be a small effect since in all practical cases the specimen can be prepared thinner than 100 nm, so multiple inelastic scattering can be neglected.

Equation (10) establishes a fundamental relationship between the coherence of a fast probe electron and the correlation function of the scatterer: The density matrix (in real space) of electrons scattered inelastically with energy loss E is the Fourier transform of Eq. (10),

$$\rho_E(\mathbf{x},\mathbf{x}') = \left(\frac{me^2\pi}{\varepsilon_0\hbar^2 k}\right)^2 FT_{\mathbf{q},-\mathbf{q}'}[Q^{-2}Q'^{-2}] * FT_{\mathbf{q},-\mathbf{q}'} \times [S(\mathbf{Q},\mathbf{Q}',E)]\,. \tag{11}$$

The convolution operator $*$ links localization and coherence of the probe to localization and correlation of charges in the scatterer.

We note in passing that Eq. (10) is the basis for calculation of channeling phenomena in inelastic scattering.[20,21]

Via Eqs. (3) and (10), we have experimental access to the correlation function, measuring the inelastic differential cross section. This is, however, problematic since the Fourier transform of the Coulomb interaction $1/q^4$ between probe and scatterer acts as a low pass filter. Noise and multiple scattering in the specimen will introduce considerable errors at higher q. In order to bypass this obstacle, it has been attempted to obtain information on the correlation of the elementary excitations from holography experiments.[15–17]

A. Electron holography

The first electron interferometer used amplitude splitting at crystals both for splitting and superimposing the electron waves.[22] A crystal can be considered an amplitude splitter in that, by diffraction, the incoming wave is split up into partial waves, which are superimposed subsequently. Later on, this principle was also used by others.[23–25]

In today's electron holography, the principle of wavefront splitting using the Möllenstedt electron biprism[26] is routinely used. The biprism is a wavefront splitter, splitting each wave $\psi(\vec{x})$ emerging from the object plane into two partial waves which are subsequently superimposed in the detector plane with a relative displacement (shear) **d**. For an overview, see, e.g., Ref. 27.

We assume here and in the following that the lens system is aberration-free. Assume that a single exit wave $\psi(\vec{x})$ is defined over the entire object plane. The biprism induces a relative shift **d** between two partial images. Consequently, in the detector plane the wave function is a superposition of the two partial waves emerging at $\mathbf{x}-\mathbf{d}/2$, and at $\mathbf{x}+\mathbf{d}/2$,

$$\psi(\mathbf{x}) = \psi(\mathbf{x}-\mathbf{d}/2)e^{i\mathbf{k}_c/2\mathbf{x}} + \psi(\mathbf{x}+\mathbf{d}/2)e^{-i\mathbf{k}_c/2\mathbf{x}}, \tag{12}$$

where $\mathbf{k}_c = k\beta\mathbf{e}_d$ is the carrier frequency of the interference fringes proportional to the superposition angle $\pm\beta$ induced by the biprism to the two partial waves. The unit vector $\mathbf{e}_d$ is perpendicular to the axis of the biprism (parallel to **d**).

After squaring, one finds the interference pattern

$$I(\mathbf{x}) = I(\mathbf{x}-\mathbf{d}/2) + I(\mathbf{x}+\mathbf{d}/2) + 2\,\mathrm{Re}[\psi(\mathbf{x}-\mathbf{d}/2)\psi^*(\mathbf{x}+\mathbf{d}/2)e^{i\mathbf{k}_c\cdot\mathbf{x}}]. \tag{13}$$

The last (interference) term can be written alternatively as $2|\psi(\mathbf{x}-\mathbf{d}/2)\psi^*(\mathbf{x}+\mathbf{d}/2)|\cos[\mathbf{k}_c\mathbf{x}+\Delta\phi(\mathbf{x},\mathbf{d})]$. Here, $\Delta\phi$ is the phase shift between waves emerging at points $\mathbf{x}-\mathbf{d}/2$ and $\mathbf{x}+\mathbf{d}/2$.

B. Partially coherent illumination

We assume that the object is illuminated by a monochromatic, extended source. A point at $\mathbf{r}_s$ in the source contributes intensity $i_s(\mathbf{r}_s)$ and induces an additional phase shift $e^{i\gamma(\mathbf{r}_s,\mathbf{x})}$ to the object exit wave, where γ depends on the action taken between source and object.[39] When we integrate over $\mathbf{r}$ in the correspondingly changed Eq. (13), the intensity terms remain unchanged since the phases γ cancel, and the interference term becomes

$$2\,\mathrm{Re}[\psi^*(\mathbf{x}-\mathbf{d}/2)\psi(\mathbf{x}+\mathbf{d}/2)e^{-i\mathbf{k}_c\cdot\mathbf{x}}\mu_{sc}(\mathbf{d})],$$

where we have used the fact that the integral over the source illumination function $i_s(\mathbf{r}_s)$ is the spatial coherence

$$\mu_{sc}(\mathbf{d}) = \int i_s(\mathbf{r}_s)e^{i[\gamma(\mathbf{r}_s,\mathbf{x}+\mathbf{d}/2)-\gamma(\mathbf{r}_s,\mathbf{x}-\mathbf{d}/2)]}d^2r_s. \tag{14}$$

In the far-field approximation, the Fresnel propagator appearing in Eq. (14) degenerates to the Fourier transform operator, and $\mu_{sc}(d)=FT_{\vec{r}_s}[i_s]$. Usually, in electron microscopy the source is assumed to be rotationally symmetric; hence $\mu_{sc}=\mu_{sc}(d)$ is real. More generally, the partial coherence function should also include temporal coherence, which can usually be neglected since the energy spectrum is narrow. In this case, we can write

$$\boldsymbol{I}(\mathbf{x}) = I(\mathbf{x}-\mathbf{d}/2) + I(\mathbf{x}+\mathbf{d}/2) + 2\mu_{sc}(d) \times|\psi(\mathbf{x}-\mathbf{d}/2)\psi^*(\mathbf{x}+\mathbf{d}/2)|\cos\left[\mathbf{k}_c\mathbf{x} + \Delta\phi(\mathbf{x},\mathbf{d})\right]. \tag{15}$$

The two superimposed waves have a degree of spatial coherence μ_{sc}. Both β and shear d are proportional to the applied biprism voltage with a proportionality factor given by the geometry of the setup. Spatial coherence of illumination can be determined by measuring the contrast for different shear (i.e., changing the biprism voltage).[28]

If one partial wave runs entirely through vacuum and the other one through an object, the elastic interaction (without any energy transfer) in general results in a modulation of amplitude and phase with respect to vacuum. The first partial wave is then given as $\psi_{vac}=1$ and the second one as $|\psi_{obj}|e^{i\Delta\phi}$. Assuming that the specimen occupies the positive half-space of the object plane (its edge passing through $\vec{x}=0$, perpendicular to $\vec{d}$), the interferogram Eq. (15) reads

$$I(\mathbf{x}) = 1 + I_{obj}(\mathbf{x}+\mathbf{d}/2) + 2\mu_{sc}(\vec{d})|\psi_{obj}(\mathbf{x}+\mathbf{d}/2) \times|\cos\left[\mathbf{k}_c\mathbf{x} + \Delta\phi(\mathbf{x},\mathbf{d}/2)\right], \tag{16}$$

where the mean fringe contrast is still given by the degree of coherence of illumination. Such interferograms give rise to all sorts of applications in electron interferometry and holography; for a review, see Ref. 27.

C. Inelastic holography

It has been shown[29] that the interference fringes produced by superposition of waves inelastically scattered with energy loss δE with the vacuum reference wave disappear in the record, when the recording time obeys

$$\tau > h/\delta E.$$

Since τ is of the order of seconds, the limiting energy loss is about 10^{-15} eV. In a way, the biprism is a perfect energy filter.

If both waves have suffered the same energy loss, the fringes would reappear only if phase coherence is given. In order to study phase coherence, it is therefore reasonable to bring two waves with the same energy loss from different positions in the specimen to interference. Since elastic holography detects phase relations between different points, it can be anticipated that the same is true for inelastic holography. Any nonarbitrary phase relation between waves emerging from different points of the scatterer could be detected. This would then be an elegant pathway to study the correlation in solid state excitations. Since it has been argued that ionization is a very localized process, one would not expect correlations between points at a larger distance than the atomic scale. On the other hand, plasma excitations seem a good candidate for inelastic holography since they are collective throughout the medium. The decisive criterion is then whether the interaction processes preserve phase coherence between the two waves.

Experimentally, the question was tackled in an electron microscope equipped with an energy filter. Both waves were run through adjacent areas of the same object, hence offering the same inelastic interactions to the beam electrons. Indeed, interference fringes with sufficient contrast were found when selecting the Al-plasmon loss by the energy filter.[15,16] In the latter experiment, by means of the biprism voltage, the lateral distance d (shear) was made as large as 10 nm without losing the contrast in electron noise. This means that the radius of a coherence patch in the outgoing wavefield is at least 10 nm wide.

What is measured in this experiment is the mutual coherence function[30] of electrons in the exit plane of the specimen having suffered a plasmon loss.

In analogy to the elastic case Eq. (13), one could argue that the hologram reads

$$I(\mathbf{x}) = I(\mathbf{x}-\mathbf{d}/2) + I(\mathbf{x}+\mathbf{d}/2) + 2\mu_{sc}(\mathbf{d}) \times\mathrm{Re}[\psi_E(\mathbf{x}-\mathbf{d}/2)\psi_E^*(\mathbf{x}+\mathbf{d}/2)e^{i\mathbf{k}_c\cdot\mathbf{x}}]. \tag{17}$$

The essential question is whether the relative phase between the two partial interfering waves ψ_E of inelastically scattered electrons at positions $\mathbf{x}-\mathbf{d}/2$ and $\mathbf{x}+\mathbf{d}/2$ is fixed as in the elastic case, or arbitrary. If it is arbitrary, it would induce a new kind of (inelastic) incoherence. In this case, it would be necessary to average the interference term in Eq. (17) in order to write

$$I(\mathbf{x}) = I(\mathbf{x}-\mathbf{d}/2) + I(\mathbf{x}+\mathbf{d}/2) + 2\langle\mu_{out}(\mathbf{d})\rangle\cos\left[\mathbf{k}_c\mathbf{x} + \Delta\phi(\mathbf{x},\mathbf{d})\right]$$

with an averaged mutual coherence function of the outgoing electrons,

$$\langle\mu_{out}(\mathbf{d})\rangle = \mu_{sc}(\mathbf{d})\langle\psi_E(\mathbf{x}-\mathbf{d}/2)\psi_E^*(\mathbf{x}+\mathbf{d}/2)\rangle.$$

It is difficult to imagine how the wave function after inelastic scattering should enter this averaging process, and how the phase shift $\Delta\phi(\mathbf{x},\mathbf{d})$ should be obtained.

A closer inspection shows that this is indeed the weak point because, after inelastic interaction with energy loss E, the probe electron is not in a pure state any longer. Rather, it is entangled with the specimen's electrons. This means that it can no longer be described by a wave function.

The proper tool for describing mixed states is the density matrix.[40,31] We build the intensity of the mixed state as the sum over the individual exit wave functions which contribute to a given energy loss, with Eq. (12),

$$I_E(\mathbf{x}) = \sum_j|\psi_j(\mathbf{x}-\mathbf{d}/2)|^2 + \sum_j|\psi_j(\mathbf{x}+\mathbf{d}/2)|^2 + 2\,\mathrm{Re}\left[\sum_j\psi_j(\mathbf{x}-\mathbf{d}/2)\psi_j^*(\mathbf{x}+\mathbf{d}/2)e^{i\mathbf{k}_c\cdot\mathbf{x}}\right]. \tag{18}$$

With the substitutions

$$\bar{\mathbf{x}} = \frac{\mathbf{x}+\mathbf{x}'}{2},$$

$$\mathbf{d} = \mathbf{x}-\mathbf{x}',$$

and the inelastic density matrix for probe electrons after energy loss E,

$$\rho_E(\mathbf{x},\mathbf{x}') = \sum_j \psi_j(\mathbf{x})\psi_j^*(\mathbf{x}'),$$

this can be written as

$$I_E(\bar{\mathbf{x}}) = \rho_E(\mathbf{x},\mathbf{x}) + \rho_E(\mathbf{x}',\mathbf{x}') + 2\,\mathrm{Re}[\rho_E(\mathbf{x},\mathbf{x}')e^{i\mathbf{k}_c\cdot\bar{\mathbf{x}}}]. \quad (19)$$

The coherence of the incident wave field can be included exactly as in Eq. (15) for the elastic case, integrating over the source area. Equation (18) is then

$$I_E(\bar{\mathbf{x}}) = \rho_E(\mathbf{x},\mathbf{x}) + \rho_E(\mathbf{x}',\mathbf{x}') + 2\mu_{sc}(\mathbf{d})\mathrm{Re}[\rho_{\mathbf{E}}(\mathbf{x},\mathbf{x}')e^{i\mathbf{k}_c\cdot\bar{\mathbf{x}}}]. \quad (20)$$

For a pure state, Eq. (19) would simplify to Eq. (17). Indeed, the difference is in the interference term which is now an off-diagonal element of the density matrix, multiplied with the carrier frequency and the coherence of the incident wave field.

Equation (20) is the fundamental equation. It is a natural extension of the pure state description to an arbitrary number of (incoherently) superposed wave functions, and is as such well adapted to the case of inelastic scattering.

For isotropic scattering, the density matrix ρ_E is real, so

$$I_E(\bar{\mathbf{x}}) = \rho_E(\mathbf{x},\mathbf{x}) + \rho_E(\mathbf{x}',\mathbf{x}') + 2\mu_{sc}(\mathbf{d})\rho_{\mathbf{E}}(\mathbf{x},\mathbf{x}')\cos(\mathrm{k}_c\cdot\bar{\mathbf{x}}). \quad (21)$$

We can now redefine the mutual coherence function of the outgoing wave field as

$$\mu_{out}(\mathbf{x},\mathbf{x}') = \mu_{sc}(\mathbf{x}-\mathbf{x}')\rho_E(\mathbf{x},\mathbf{x}') \quad (22)$$

(when we consider these quantities as matrices, this is the "dot" product of the incident electron's coherence and the inelastic density matrix) and write Eq. (21) as

$$I_E(\mathbf{x}) = \rho_E(\mathbf{x},\mathbf{x}) + \rho_E(\mathbf{x}',\mathbf{x}') + 2\mu_{out}(\mathbf{x},\mathbf{x}')\cos(\mathbf{k}_c\cdot\bar{\mathbf{x}}). \quad (23)$$

The solid state plasma can be considered as homogeneous and isotropic. In this case, the density matrix in Eq. (21) depends only on the difference $|\mathbf{d}|$ of the two variables [the main diagonal value, i.e., the density, is constant, $\rho_E(\mathbf{x},\mathbf{x}) = \rho_E(0,0)$]. The mutual coherence function Eq. (22) simplifies to

$$\mu_{out}(d) = \mu_{sc}(d)\rho_E(0,d)$$

and the measured intensity is

$$I_E(\mathbf{x}) = 2\rho_E(0,0) + 2\mu_{out}(d)\cos(\mathbf{k}_c\cdot\mathbf{x}). \quad (24)$$

The amplitude of the fringes measures the off-diagonal element of the inelastic density matrix $\rho_E(0,d)$, which, in turn, is identical to the mutual object transparency for energy loss E, introduced by Rose.[32] A good description of image formation both for potential scattering and for inelastic interactions, based on the mutual coherence function and mutual object transparency, is the treatment of Müller *et al.*[33] The fringe contrast in the inelastic hologram is given in terms of the mutual object transparency μ_{out} as

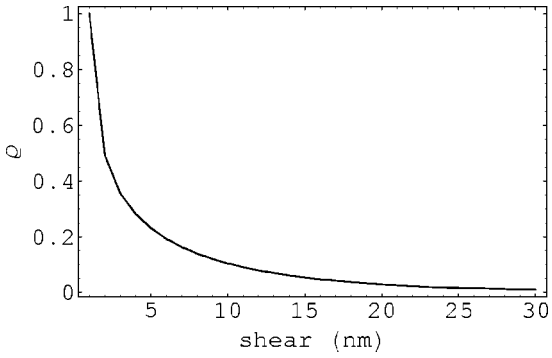

FIG. 2. Off-diagonal density-matrix element (mutual coherence) $\rho_E^h(0,d)$ of electrons emerging from the exit plane of an infinitely extended homogeneous Al specimen, after excitation of a plasmon, as a function of holographic shear.

$$\frac{I_{max}-I_{min}}{I_{max}+I_{min}} = \frac{\mu_{out}(d)}{\rho_E(0,0)}. \quad (25)$$

In complete analogy to potential scattering, we can then relate the fringe contrast to the mutual coherence function. Therefrom, the off-diagonal term of the density matrix of the inelastically scattered electron can be easily obtained from a hologram.

Predicting fringe contrast needs the calculation of $\rho_E(0,d)$. Quite generally, for an arrangement of scatterers with spatial distribution $g(\mathbf{r})$, the total density matrix is

$$\rho_E^t(\mathbf{x},\mathbf{x}') = \int g(\mathbf{r})\rho_E(\mathbf{x}-\mathbf{r},\mathbf{x}'-\mathbf{r})d^2r.$$

For a homogeneous infinitely extended system, the total density matrix can be found analytically by integrating the mixed dynamic form factor in the dipole approximation over all independent scattering centers at $\mathbf{r}$ with proper phase shifts,

$$S^h(\mathbf{Q},\mathbf{Q}',E) \propto \int \mathbf{Q}\cdot\mathbf{Q}'e^{i(\mathbf{q}-\mathbf{q}')\cdot\mathbf{r}}\,d^2r \propto \mathbf{Q}\cdot\mathbf{Q}'\;\delta^2(\mathbf{q}-\mathbf{q}'). \quad (26)$$

The corresponding density matrix is obtained as the Fourier transform of Eq. (26),

$$\rho_E^h(\mathbf{x},\mathbf{x}') = FT_{\mathbf{q},-\mathbf{q}'}\left[\frac{S^h(\mathbf{Q},\mathbf{Q}',E)}{Q^2Q'^2}\right] = \int_0^{q_c} Q^{-2}e^{i\mathbf{q}\cdot(\mathbf{x}-\mathbf{x}')}d^2q$$

$$= \int_0^{q_c} qJ_0(q|\mathbf{x}-\mathbf{x}'|)Q^{-2}dq \quad (27)$$

with the Bessel function of first kind and zero order J_0. The function $\rho_E^h(0,d)$ is shown in Figs. 2 and 3 for the Al plasmon. It can be interpreted as the contrast of fringes as a function of shear d for perfectly coherent illumination.[34] The 10% level is reached at a shear of 9.1 nm, and at 20 nm we find 0.026, both in good agreement with the interference experiments of Lichte and co-workers.[16,17]

We can now compare the mutual coherence function with the correlation function in the Al plasmon, Eq. (5). Figure 4

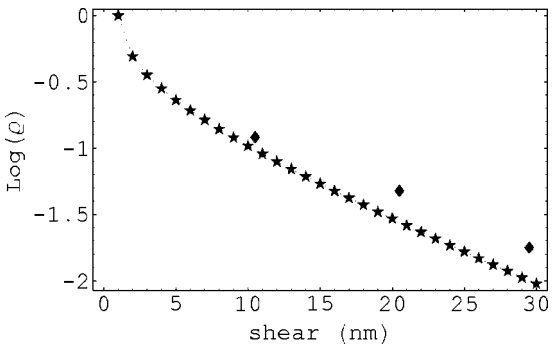

FIG. 3. Same as in Fig. 2 on a logarithmic scale, compared with experimental values (♦) (Ref. 35).

shows the first 2 nm together with the 2D correlation function. The mutual coherence function is smoothly decreasing; it is so broad because of the long-range Coulomb interaction between target charges and the probe electron. The faint wiggles at the first few nm are remnants of the strong oscillations in the correlation function.

V. PROPOSAL FOR EXPERIMENTS

The coherence function Eq. (27) can be approximated by the truncated Bessel function, which we define in terms of the Bessel function of the second kind and zeroth-order K_0 as

$$K_0^t(x) = \begin{cases} 1, & x < 1/q_c \\ K_0(q_E x)/\ln(q_c/q_E) & \text{otherwise} \end{cases} \tag{28}$$

It has been shown[8] that the intensity of a pointlike scatterer decays as $K_0^t(q_e\,x)^2$ with distance from the excitation. Since the coherence function decays as $K_0^t(q_e\,x)$, one might expect unusual behavior of the holographic fringe contrast,

$$\frac{\rho_E(0,d)}{\rho_E(0,0)} \propto \frac{1}{K_0^t(q_e\,d)} \tag{29}$$

in the vicinity of localized excitations. Equation (29) predicts increasing fringe contrast with increasing distance from the excitation.

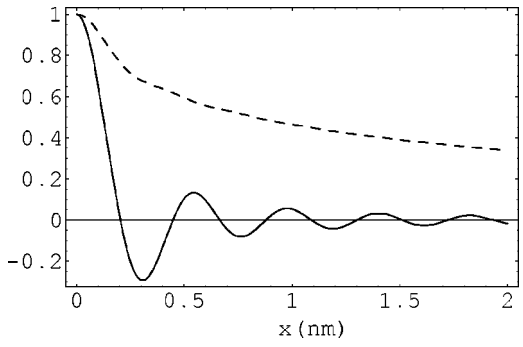

FIG. 4. Dashed line: Off-diagonal density-matrix element (mutual coherence) $\rho_E^h(0,d)$ of electrons, compared with the two-dimensional projection of the density correlation function of the scatterer, Eq. (5) (full line), as a function of shear.

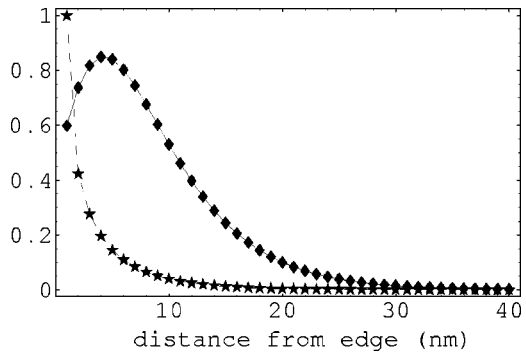

FIG. 5. Intensity (dashed) and mutual coherence $\rho_E^h(\mathbf{x},\mathbf{x}+\mathbf{d})$ (♦) outside of an Al specimen as a function of distance from the border. The shear is 20 nm parallel to the edge of the specimen. Both curves are normalized to intensity 1 at the edge. The mutual coherence is enlarged by a factor of 50.

In the following, we apply the outlined theory in two cases, using the inelastic density matrix for the calculation of (a) the inelastic mutual coherence outside an excited medium, and (b) we predict reversal of the fringe contrast in the vicinity of a small isolated area of excitation. The first result is unexpected and could be tested by holography. The second result is even more surprising because it would show, directly, a phase shift of π in inelastic scattering.[41]

A. Plasmon coherence in vacuum

The total density matrix for a distribution of scatterers filling the half-space $\mathbf{r}=(\xi>0,\eta)$ is

$$\rho_E^t(\mathbf{x},\mathbf{x}') = \int_{-\infty}^{\infty}\int_0^{\infty} g(\mathbf{r})\rho_E(\mathbf{x}-\mathbf{r},\mathbf{x}'-\mathbf{r})d\xi d\eta. \tag{30}$$

Numerical integration yields the intensity profile and the coherence function as shown in Fig. 5.

Note the decrease in the mutual coherence close to the border of the specimen. This is a consequence of the negative contributions to the density matrix for distances that are small with respect to the shear.

The fringe contrast Eq. (25) is shown in Fig. 6 as a function of distance from the edge. It is seen that the contrast increases outside the scattering medium. This surprising behavior can be attributed to the faster decrease of the intensity (which behaves approximately as K_0^2) with respect to the coherence function. At the very edge of the specimen, the contrast is 0.012, whereas in the medium (far from the edge), Eq. (28) predicts 0.025. That means that we should see a small dip in contrast when we approach the specimen's border from the inside.

B. Contrast reversal in small excited areas

Assume a pointlike scatterer. When we impose a shear d by the biprism, we will see the source of inelastic scattering overlapping with the shifted second image. Since the intensity decreases smoothly outside the inelastic source and its image, we will also detect the tails of the second (virtual) source.

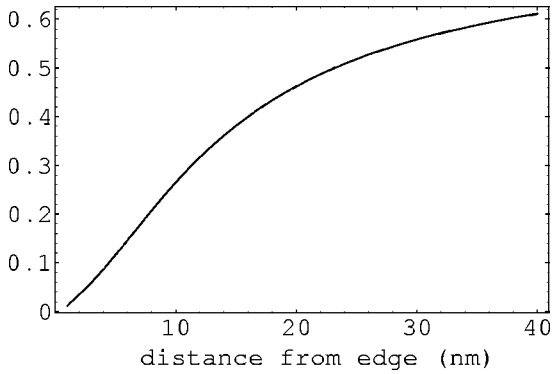

FIG. 6. Predicted fringe contrast outside of the Al specimen for a shear of 20 nm parallel to the edge of the specimen.

In the dipole approximation, it is found that the density matrix of the inelastically scattered electrons is

$$\overline{\rho}_E(\mathbf{x},\mathbf{x}') = v(x)v(x')\,\mathbf{e}_x \cdot \mathbf{e}_{x'} + w(x)w(x'). \tag{31}$$

Here, $\mathbf{e}_x$ is a unit vector in direction $\mathbf{x}$ in the exit plane. The two functions in Eq. (31) are[8]

$$v = \frac{1}{2\pi}\int_0^\infty \frac{qJ_1(qx)f(Q)}{Q^2}dq, \tag{32}$$

$$w = \frac{q\boldsymbol{E}}{2\pi}\int_0^\infty \frac{J_0(qx)f(Q)}{Q^2}dq. \tag{33}$$

Note that the scalar product $\mathbf{e}_x \cdot \mathbf{e}_{x'} = \cos\phi$ is negative when the angle ϕ between directions $\mathbf{x},\mathbf{x}'$ is $>\pi/2$.

Therefore the density matrix $\rho_E(\mathbf{x},\mathbf{x}')$ has negative contributions, and we expect contrast inversion of the fringes (in other words, there is a phase shift of π between some partial inelastically scattered waves). The results for a shear of 20 nm are shown in Fig. 7, showing the area where the density matrix is negative (we set the positive parts to zero in the figure so as to facilitate visualization), and in Fig. 8, showing the density matrix as a density plot (white is negative, black positive) and a simulation of the fringes. Contrast inversion can be observed in the semicircular area between the source and its image. Note that both figures show only the right half-plane since everything is symmetric with respect to the line connecting source and image.

The minimum contrast is -0.37; it is found at the midpoint between the real and the virtual source. We propose therefore such an experiment with a small circle or sphere of a material with a well-defined plasmon, such as Al or Si. Apart from the difficulty to prepare a specimen with an almost pointlike excitation source surrounded by vacuum, the question is whether the intensity is high enough to detect the effect and whether the strong intensity background from the point sources does not hide the minute fringe amplitudes. A simulation for an extended source is more tricky—we think that the contrast inversion will still be visible, albeit with smaller amplitudes and in a smaller region. We expect visibility of the contrast inversion when the diameter of the excited region is well below the holographic shear.

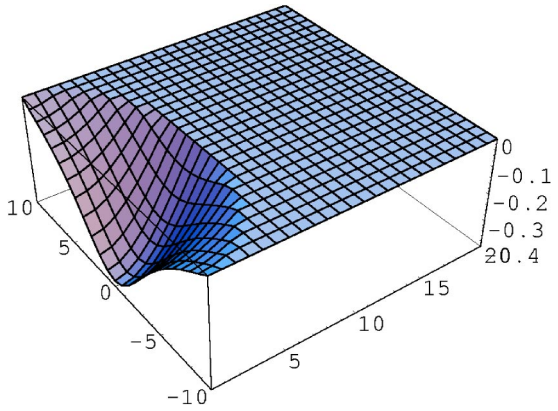

FIG. 7. Area of negative contributions to the density matrix $\rho_E(\mathbf{x},\mathbf{x}+\mathbf{d})$ of a pointlike excitation for a shear of 20 nm. The point and its image are situated at (0,10) and at $(0,-10)$

VI. CONCLUSIONS

We discussed several approaches to the correlation length in solid state plasmas. Results derived from the plasmon correlation function and its two-dimensional projection onto the plane of observation are in good agreement with earlier estimates.

It was further shown that the small correlation length in solid state plasmas does not contradict the coherence length of almost 30 nm found in inelastic interference experiments. The difference of nearly two orders of magnitude can be traced back to the long-range Coulomb interaction between probe and target electrons. So it may happen that two partial waves emerging from the specimen a distance d apart from each other have excited the same—very localized—plasmon and thus are coherent over that large distance. Details of the electronic correlation in the scatterer are found in the first few nm of the mutual coherence function. Sophisticated experiments will be needed to reveal these details.

An unexpected prediction of the density-matrix approach is that inelastic holography experiments should show increased contrast outside the specimen, and a phase shift of π in inelastic holograms of very small particles. With the presently available combination of highly coherent field emitters and energy filters in the transmission electron microscope, our predictions could probably be tested experimentally. Applications would cover the direct detection of

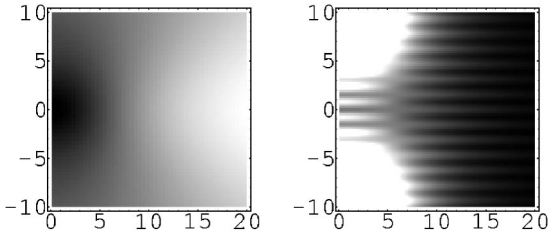

FIG. 8. Predicted fringe contrast and holographic interference fringes showing a phase shift of π in the area in between a pointlike source of inelastic scattering and its image. The pointlike source is at (0 nm,-10 nm); the shear is 20 nm in the vertical direction.

phase correlation in various excitations, including the phase shifts induced by transition to final states whose *m*-degeneracy is lifted in a magnetic field.

Note added in proof. The predicted increase of contrast in vacuum was recently found in an experiment on small hydrogen bubbles.[37] Further work is in progress.

ACKNOWLEDGMENTS

P.S. acknowledges the support of the Austrian Science Fund, Project No. P14038-PHY, and of the European Commission, Contract No. 508971 (CHIRALTEM). H.L. is grateful to Fondation Francqui, Brussels, for support of this research.

*On leave from: Institute for Solid State Physics, Vienna University of Technology, A-1040 Vienna, Austria. Electronic address: schattschneider@ifp.tuwien.ac.at

[1] N. Vast, L. Reining, V. Olevano, P. Schattschneider, and B. Jouffrey, Phys. Rev. Lett. **88**, 037601 (2002).
[2] R. DelSole, G. Adragna, V. Olevano, and L. Reining, Phys. Rev. B **67**, 045207 (2003).
[3] H. Ness and A. Fisher, Chem. Phys. **281**, 279 (2003).
[4] K. Liu, P. Avouris, R. Martel, and W. K. Hsu, Phys. Rev. B **63**, 161404(R) (2001).
[5] P. Schattschneider and B. Jouffrey, *Plasmons and Related Excitations*, in *Energy Filtering Transmission Electron Microscopy*, edited by L. Reimer, Springer Series in Optical Sciences, Vol. 71 (Springer, Berlin, 1995), pp. 151–224.
[6] H. Müller, H. Rose, and P. Schorsch, J. Microsc. **190**, 73 (1998).
[7] P. Schattschneider, *Fundamentals of Inelastic Electron Scattering* (Springer, Vienna, 1986).
[8] P. Schattschneider, M. Nelhiebel, and B. Jouffrey, Phys. Rev. B **59**, 10 959 (1999).
[9] D. Pines, *Elementary Excitations in Solids* (W. A. Benjamin, New York, 1964).
[10] I. Egri, Z. Phys. B: Condens. Matter **53**, 183 (1983).
[11] I. Egri, Phys. Rep. **119**, 363 (1985).
[12] R. Ferrell and J. Quinn, Phys. Rev. **108**, 570 (1957).
[13] S. Cheng, Ultramicroscopy **21**, 291 (1987).
[14] M. Scheinfein, A. Muray, and M. Isaacson, Ultramicroscopy **16**, 233 (1985).
[15] A. Harscher, H. Lichte, and J. Mayer, Ultramicroscopy **69**, 201 (1997).
[16] H. Lichte and B. Freitag, Ultramicroscopy **81**, 177 (2000).
[17] H. Lichte, P. Potapov, D. van Dyck, and P. Schattschneider, in *Microscopy and Microanalysis* (Cambridge University Press, Cambridge, 2003), Vol. 9, Suppl. 3, p. 084.
[18] S. L. Dudarev, L. M. Peng, and M. J. Whelan, Phys. Rev. B **48**, 13 408 (1993).
[19] H. Kohl and H. Rose, Adv. Electron. Electron Phys. **65**, 173 (1985).
[20] P. Schattschneider, C. Hébert, and B. Jouffrey, Ultramicroscopy **86**, 343 (2001).
[21] P. Schattschneider and B. Jouffrey, Ultramicroscopy **96**, 453 (2003).
[22] L. Marton, Phys. Rev. **85**, 1057 (1952).
[23] G. Pozzi, Optik (Stuttgart) **65**, 77 (1983).
[24] F. Zhou, E. Plies, and G. Moellenstedt, Optik (Stuttgart) **98**, 95 (1995).
[25] B. M. Mertens, M. Overwijk, and P. Kruit, Ultramicroscopy **77**, 1 (1999).
[26] G. Moellenstedt and H. Dueker, Z. Phys. **145**, 377 (1956).
[27] H. Lichte, Philos. Trans. R. Soc. London, Ser. A **360**, 897 (2002).
[28] R. Speidel and D. Kurz, Optik (Stuttgart) **49**, 173 (1977).
[29] D. van Dyck, H. Lichte, and J. Spence, Ultramicroscopy **81**, 187 (2000).
[30] P. Hawkes, *Coherence in Electron Optics* (Academic Press, London, 1987), Vol. 7, p. 101.
[31] J. von Neumann, Nachr. Ges. Wiss. Goettingen, Math.-Phys. Kl. **1**, 245 (1927).
[32] H. Rose, Optik (Stuttgart) **45**, 139 (1976).
[33] H. Müller, H. Rose, and P. Schorsch, J. Microsc. **190**, 73 (1998).
[34] P. Schattschneider and B. Jouffrey, Eur. Phys. J. B **37**, 3 (2004).
[35] J. Verbeeck, Ultramicroscopy (to be published).
[36] P. Schattschneider, M. Nelhiebel, H. Souchay, and B. Jouffrey, Micron **31**, 333 (2000).
[37] P. Potapov (unpublished).
[38] This is because the angular distribution functions in inelastic scattering all have a cutoff, contrary to the Lorentzian which is infinitely extended.
[39] For free space propagation, this is the Fresnel propagator exp $\times(-i\pi[(\mathbf{r}-\mathbf{x})^2/\lambda z])$ which tends to the Fourier transform operator $\exp[-2\pi i\mathbf{r}\mathbf{x}/z]$ for $z\to\infty$.
[40] The density matrix used in the following is the reduced one-electron density matrix of the probe electron, starting from the wave function of the entangled system.
[41] In diffraction, a similar effect was already observed.[36]